

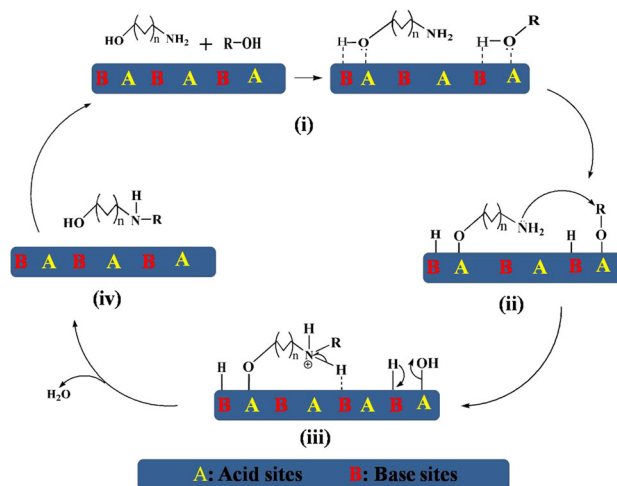
N-Alkylation of Alkylolamines with Alcohols Over Mesoporous Solid Acid–Base Cs–B–Zr Catalyst

Aimin Chen¹ · Houyong Wang¹ · Rui Liu¹ · Yingying Bo¹ · Jun Hu¹

Received: 24 February 2016 / Accepted: 23 March 2016
© Springer Science+Business Media New York 2016

Abstract The mesoporous solid acid–base Cs–B–Zr mixed oxides were synthesized using the co-precipitation method followed by a subsequent thermal treatment. The catalytic activity of solid Cs–B–Zr mixed oxide was tested for solvent free acid–base catalysed direct alkylolamines with alcohols as green alkylating agent. The effects of Cs/B/Zr ratio, calcination temperature, reaction conditions, and reaction substrate on the catalytic performance of the catalysts were investigated. The XRD, N₂ adsorption–desorption, ICP-OES, FT-IR and NH₃/CO₂-TPD results showed that the mesoporous structure and acid–base properties of the catalysts play important roles in the reaction. A suitable number of acid and basic sites on the catalyst lead to a high activity for the *N*-alkylation reaction.

Graphical Abstract A direct *N*-alkylation of amino alcohol with alcohols has been developed using mixed oxide Cs–B–Zr as an acid–base bifunctionalized catalyst.



Keywords *N*-Alkylation · Mesoporous · Acid–base catalyst · Cs–B–Zr mixed oxide

1 Introduction

N-alkylaminoalcohols are important intermediates in fine chemical industries, manufacturing, pharmaceuticals, agrochemicals, polymers and dyes, especially as desulfurizer and/or decarbonizer in environmental protection [1–3]. The production of *N*-alkylaminoalcohols is increasing with years. Traditionally, *N*-alkylaminoalcohols are mainly produced by direct alkylation by halide [4], reductive amination of methyl-carbonate/dimethyl sulfate [5–7] and ethylene oxide method [8, 9]. Nevertheless, all these processes have their own drawbacks, such as expensive reactants, low selectivity, poor yields, harsh reaction conditions and large amounts of harmful wastes polluting the

✉ Aimin Chen
amchen@zjut.edu.cn

✉ Jun Hu
hjzjut@zjut.edu.cn

¹ College of Chemical Engineering, Zhejiang University of Technology, Hangzhou 310014, China

environment. Therefore, much attention has been paid to explore a new ecologically benign synthetic route.

In the recent years, the direct *N*-alkylation of amines with alcohols has been reported as an example of “green” technology which is an alternative route through a borrowing-hydrogen (B-H) [10–12]. The advantage of this type of amination is the high atom efficiency of the reaction sequence, which forms water as the only by-product. Through a B-H process, imines are usually formed as the intermediates, and can be further reduced to alcohol amine products by the hydrogen species generated on the catalyst [13]. Since Grigg et al. and Watanabe et al. had introduced homogeneous catalysts for *N*-alkylation of amines with alcohols in 1981 for the first time [14, 15], transition metal complexes and salts such as Ru, Pd, Pt, Au and Ir catalysts have been developed as the homogeneous catalysts in the presence of solvent, promoters and bases have been reported as efficient homogeneous catalytic systems for direct *N*-alkylation of amines with alcohols [16–22]. Unfortunately, these homogeneous catalytic systems have disadvantages related to the recovery, high cost, special handling of metal complex and/or the indispensable use of co-catalysts such as bases and stabilizing agents. So, the exploration of a ligand free, base and promoter free, and solvent free heterogeneous catalytic system is highly desirable for direct *N*-alkylation of amines.

In addition to the borrowing hydrogen strategy, another approach for *N*-alkylation of amines is direct alkylation by nucleophilic substitution of alcohols using solid acids catalysts such as nanosized zeolite beta [23], Al-MCM-41 [24] and Co^{2+} -zeolites [25] and sulfated tungstate [26] which have been studied for solvent free direct *N*-alkylation amines using alcohols to establish an efficient and greener catalytic synthesis route. Recently, acid–base bifunctionalized catalysts [27–29] have attracted a great deal of attention in the field of catalysis, such as Cs–P–Si mixed oxide as a cooperative acid–base catalyst for the direct *N*-alkylation reaction with alcohols and obtained good yields in synthesizing different alkylaminoalcohols [30]. It is also found that weak acid–base pair sites played a vital role in the reaction; however, high catalytic activity and selectivity were obtained only under the supercritical fluids state. As known to all, ZrO_2 with the multiphase crystal structure, high thermal stability and amphoteric properties is widely applied in catalysis [31]. Furthermore, the acid–base properties of catalyst could be varied by doping acidic/alkaline oxide to facilitate the ability of adsorbing organic molecules [32, 33].

In this work, the solid acid–base Cs–B–Zr mixed oxides with mesoporous structure were synthesized using the coprecipitation method followed by a subsequent thermal

treatment. A typical procedure for alcohol amines *N*-alkylation reaction with alcohols was investigated to evaluate the catalytic performance of Cs–B–Zr catalyst. The activity and selectivity of these new catalysts were correlated with the results of NH_3/CO_2 -TPD measurements. In addition, the mechanism of Cs–B–Zr catalysts for direct *N*-alkylation of *N*-alkylaminoalcohol with alcohols was discussed.

2 Experimental Section

2.1 Preparation of the Catalysts

The Cs–B–Zr mixed oxide catalyst was prepared by a two-step process method with the following procedure. Firstly, 22.5 g $\text{ZrOCl}_2 \cdot 8\text{H}_2\text{O}$ was dissolved in 100 ml distilled water to which aqueous ammonia (25 %) was added dropwise with constant stirring till the solution became alkaline (pH 10) and zirconium hydroxide precipitated as white solid. A mixed solution containing 3.7 g H_3BO_3 , 11.7 g CsNO_3 and 5.1 g CTAB in 100 ml distilled water were then added to the solution obtained above with constant stirring to obtain a slurry. The resulting slurry was aged overnight in the mother liquor. Then, the resultant solution was filtered and the residue was washed with distilled water till free from chloride ions. The obtained powders were dried in an oven at 100 °C for 5 h and calcined at various temperatures (in the range of 450–750 °C) for 6 h in ambient air. The molar ratio of $\text{ZrOCl}_2 \cdot 8\text{H}_2\text{O}:\text{H}_3\text{BO}_3:\text{CsNO}_3:\text{CTAB}$ is 1:X:1:0.2, where X represents the added amount of H_3BO_3 , it was taken as 0.5, 1.0, 1.5, and 2.0, respectively. The synthesized samples using molar ratio of Cs:B:Zr = 1:0.5:1, 1:1:1, 1:1.5:1 and 1:2:1 are denoted as Cs–B–Zr/0.5, Cs–B–Zr/1, Cs–B–Zr/1.5 and Cs–B–Zr/2, respectively.

2.2 Characterizations

XRD patterns were recorded on an X’Pert PRO X-ray diffractometer produced by Dutch PANalytical company ($\text{CuK}\alpha$ radiation $\lambda = 0.1541$ nm, 40 kV, 40 mA) with a scan speed of 8°/min and a scan range of 1°–10° and 17°–80°. The nitrogen adsorption–desorption was performed by using an ASAP 2020 Micromeritics, USA, after the degassing of samples under vacuum (–0.1 MPa) at 200 °C for 3 h, measurements at –196 °C. Surface area was determined by Brunauer–Emmett–Teller (BET) equation. The pore-size distribution, based on the desorption branch of the isotherm, was estimated using the method developed by Barret, Joyner, and Halender (BJH), assuming a cylindrical

pore modal. The inductively coupled plasma-optical emission (ICP-OES) spectrophotometer (Optima 2000DV, Perkin–Elmer, Eden Prairie, MN) was used to determine the composition and the doping amount of element in the synthesized materials. The sample material was digested in concentrated HF and diluted with water. A scanning electron microscope (SEM) equipped with HIT S-4700 was used to detect the morphology of samples. Transmission electronic microscope (TEM) images were acquired by using a Philips-FEI Tecnai G2F30 S-Twin microscope. FT-IR was detected by Nicolet205 type Fourier transform infrared spectrometer. NH_3/CO_2 -TPD measurements were conducted by using a Micromeritics Au-tochem-II instrument, and for this 200 mg of Catalyst sample was placed in a U shaped sample tube. The sample was pre-treated in helium ($40 \text{ cm}^3 \text{ min}^{-1}$) for 0.5 h at $250 \text{ }^\circ\text{C}$ then cooled down to $100 \text{ }^\circ\text{C}$. NH_3 and CO_2 gases were used to study acidic and basic strength respectively. Corresponding gas was adsorbed on the sample for 1 h under 1.33 MPa. The physisorbed gas was removed by flashing the samples with helium for 30 min. TPD measurements were conducted in the temperature range from 100 to $700 \text{ }^\circ\text{C}$. The graph was recorded using a TCD detector.

2.3 Catalytic Activity Measurements

N-Alkylation reaction was performed in a volume of 500 ml stainless-steel autoclave batch reactor. A mixture of 2-aminoethanol (0.5 mol) with methanol (1.5 mol) was added to the reactor containing 4 wt% of catalyst (with respect to 2-aminoethanol). The N-alkylation reaction was conducted under the constant stirred with a speed 200 r min^{-1} at $220 \text{ }^\circ\text{C}$ and 4.3 MPa (To maintain the pressure in the reaction kettle by adding nitrogen) for 35 min. The reaction products were identified by GC–MS analysis (Agilent 5973N-6890N, Agilent Technologies). The selectivity and chemical conversions of the products were determined by GC analysis (GC-17A, Shimadzu Co; FID detector and DB-1 ms capillary column, J&W). The conversion of amino alcohol was calculated on the basis of its weight percent as follows:

$$\text{Conversion}(\%) = 100 \times \frac{\text{Initial wt\% of amino alcohol} - \text{Final wt\% of amino alcohol}}{\text{Initial wt\% of amino alcohol}}$$

The selectivity of the product was calculated as:

$$\text{Selectivity}(\%) = 100\% \times \frac{\text{Peak area of product}}{\sum \text{Total Peak area for all the products}}$$

Qualitative analysis was compared with standard chromatographic and mass spectrometry of the product.

3 Results and Discussion

3.1 XRD of Catalysts

Figure 1a showed wide-angle XRD patterns of ZrO_2 , B–Zr and Cs–B–Zr/1. The pattern of ZrO_2 which calcined at $550 \text{ }^\circ\text{C}$, presented a pure tetragonal crystalline phase (JCPDS, CAS No. 00-014-0534). With the introduction of borate, the peaks in the B–Zr and Cs–B–Zr/1 were lower and broader than pure ZrO_2 which indicated that

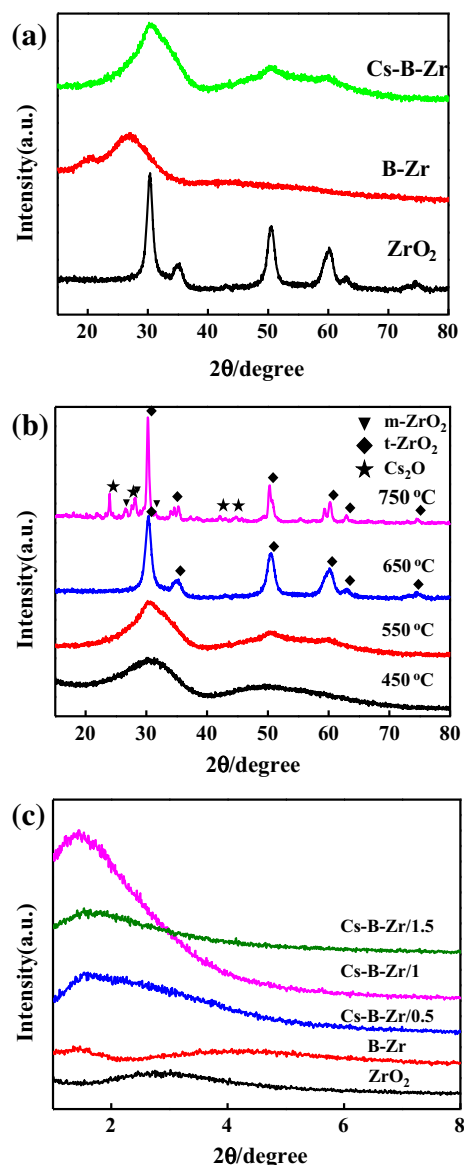


Fig. 1 a Wide angle XRD patterns for the synthesized samples calcined at $550 \text{ }^\circ\text{C}$. b Wide angle XRD patterns for the synthesized Cs–B–Zr/1 mixed oxide calcined at various temperatures. c Small angle XRD patterns for the synthesized samples calcined at $550 \text{ }^\circ\text{C}$ for 6 h

amorphous state and low crystal morphology were formed in the framework of B–Zr and Cs–B–Zr/1, respectively. It could be attributed to the smaller particles and grain size in the structure of B–Zr and Cs–B–Zr/1. Previous studies found that with incorporation of the borate ion in the ZrO₂ system suppressed the crystallization and led to the formation of poor crystal structure and smaller particle size materials [32]. Figure 1b presented the XRD patterns of Cs–B–Zr/1 sample at different calcined temperatures. The broad nature of these diffraction spectra at 450 and 550 °C suggested the low crystalline nature in the structure of samples. With the rising of temperature, the crystallinity of the sample was increased and typical diffraction peaks for tetragonal metastable t-ZrO₂ were appeared. The diffraction peaks of Cs–B–Zr/1 at 750 °C were added with several new peaks at 25.93°, 28.22°, 42.52° and 45.42°, which were assigned to hexagonal phase of Cs₂O (JCPDS, CAS No. 00-09-0104). While the new peaks at 23.98°, 28.08° and 31.32° were assigned to monoclinic m-ZrO₂ crystalline phase, namely, a polycrystalline phase was formed in the Cs–B–Zr/1 sample. Figure 1c showed small angle XRD diffraction patterns of mixed oxide samples and ZrO₂. The Cs–B–Zr/1 sample calcined at 550 °C showed an obvious single broad peak at around $2\theta = 1.9^\circ\text{--}3.5^\circ$ which implied the formation of mesoporous in the Cs–B–Zr mixed oxide.

3.2 ICP and BET Analysis of Catalysts

Figure 2 showed the N₂ adsorption–desorption isotherm and pore size distribution of Cs–B–Zr mixed oxide calcined at 550 °C. The N₂ isotherm for Cs–B–Zr/1 presented three adsorption stages ($P/P_0 < 0.2$, $0.2 < P/P_0 < 0.7$ and $P/P_0 > 0.7$). Based on the IUPAC classification, the

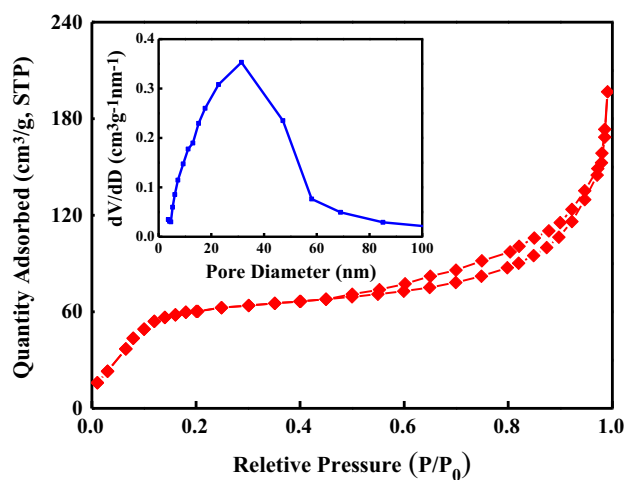


Fig. 2 N₂ adsorption–desorption isotherm. The *inset* is the corresponding pore-size distribution of Cs–B–Zr/1 mixed oxide calcined at 550 °C

isotherms for these materials could be categorized as type I with borderline type V characteristics and a type H3 hysteresis loop, indicating the presence of mesoporous structure [34, 35] with a pore size distribution at 5–50 nm. Furthermore, type H3 hysteresis were usually only observed on solids containing aggregates or agglomerates of particles, which could lead to slit-shaped pores that were non-uniform in size and shape. The composition and textural properties of the different catalysts were summarized in Table 1. From the ICP results, the molar ratios of Cs:B:Zr in the catalysts determined by chemical analysis were close to those added in the reactant mixtures during the synthesis. The incorporation of B and Cs into the mixed oxide catalyst system also resulted in significant improvements in surface area. The Cs–B–Zr/1 showed the largest surface area ($A_{\text{BET}} = 227 \text{ m}^2 \text{ g}^{-1}$). When increasing doping amount of boron, Cs–B–Zr/1.5 and Cs–B–Zr/2 samples showed smaller surface areas (189 and $152 \text{ m}^2 \text{ g}^{-1}$) than Cs–B–Zr/1 and the average pore diameter decreased from 21 to 31 nm. It is believed that the excess boric acid decomposed to form boron oxide particles, and the pores were blocked by the boron oxide particles which led to the decreasing of the surface and the pore size of the catalyst [36, 37].

3.3 Textural and Surface Properties of Catalysts

Figure 3 showed the SEM and TEM images of Cs–B–Zr/1 mixed oxide calcined at 550 °C. As shown in Fig. 3a, the SEM of the Cs–B–Zr/1 sample revealed the presence of uniform spherical particles structure on the surface of the catalyst with an average diameter in the range of 30–40 nm. The TEM image in Fig. 3b demonstrated that the existence of worm-like pores in the spherical particles and uniformly dispersed on the catalyst surface.

3.4 FT-IR Spectra of Synthesized Oxides

Figure 4 showed the FT-IR spectra of ZrO₂, Cs–B–Zr/1 and B–Zr calcined at 550 °C. The IR spectra of samples Cs–B–Zr/1 and B–Zr showed strong absorption bands in the range of 1290–1440 cm⁻¹ with a peak at 1379 cm⁻¹, corresponding to tetrahedral [BO₄] unit. Simultaneously, the peaks at 1190 cm⁻¹ were assigned to trigonal [BO₃] unit [38, 39], which confirmed that two units (tetrahedral BO₄ and trigonal BO₃) existing in the synthesized Cs–B–Zr/1 [40]. The peaks at 1005 and 900 cm⁻¹ in the synthesized Cs–B–Zr/1, which was absent in the spectrum of pure ZrO₂ and B–Zr mixed oxide were assigned to characteristic peaks of Cs₂O [33]. In addition, the peak at 3424 and 1626 cm⁻¹ in all samples were assigned to the stretching and bending vibration of hydroxyl groups and water molecules. In the spectrum of ZrO₂, two

Table 1 The composition and textural properties of the different catalysts

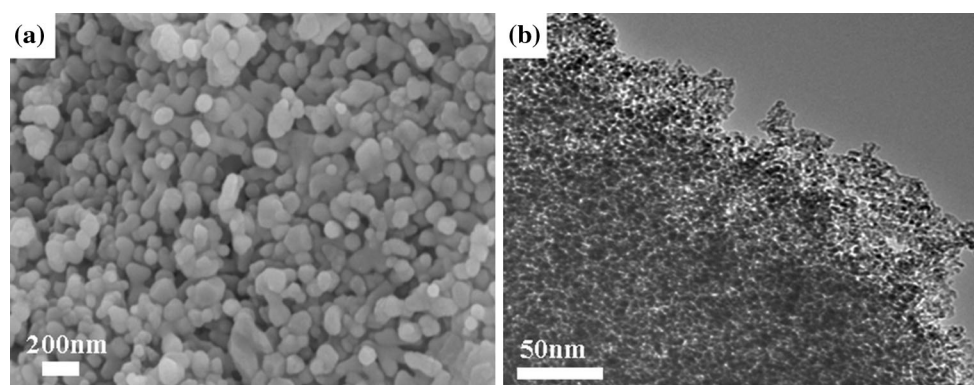
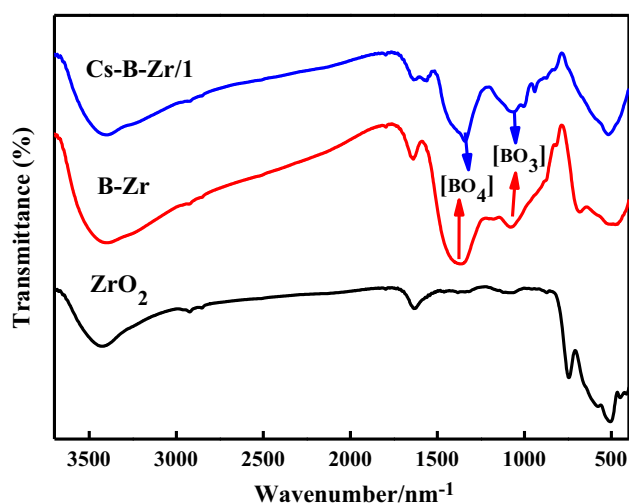
Entry	Samples	Cs:B:Zr ^a	A _{BET} (m ² g ⁻¹) ^b	V (m ³ /g) ^c	D (nm) ^d
1	ZrO ₂	–	106	0.14	52.83
2	B–Zr	0.91:1	224	0.12	21.43
3	Cs–B–Zr/0.5	0.97:0.47:1	207	0.15	28.99
4	Cs–B–Zr/1	1.03:0.97:1	227	0.18	31.72
5	Cs–B–Zr/1.5	1.07:1.43:1	189	0.16	23.86
6	Cs–B–Zr/2	1.00:1.80:1	152	0.08	21.05

^a The ratio of Cs:B:Zr by ICP-OES detection under the conditions of calcination temperature at 550°

^b BET surface area

^c Single point adsorption total pore volume at P/P₀ = 0.97

^d Average pore diameter (4 V/A by BET)

**Fig. 3** Images of Cs–B–Zr/1 mixed oxide calcined at 550 °C. **a** SEM and **b** TEM**Fig. 4** FT-IR spectra of the synthesized samples calcined at 550 °C

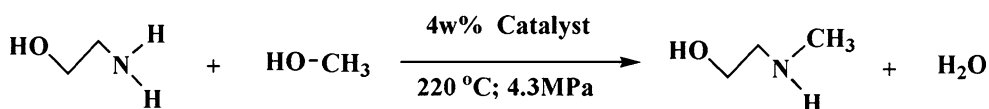
characteristic peaks at 750 and 620 cm⁻¹ were assigned to the monoclinic phase ZrO₂ [41]. However, the intensities of two bands in Cs–B–Zr/1 and B–Zr corresponding to ZrO₂ were decreased because of the existence of [BO₄] and [BO₃] units. Additionally, the bands at 3450 and

1626 cm⁻¹, assigned to physisorbed and coordinated water, were also observed.

3.5 Catalytic Activity

3.5.1 Catalytic Activity of Different Catalyst for N-alkylation of 2-Amino Ethanol with Methanol

The catalytic performance of the reaction of 2-aminoethanol with methanol was tested using 4 wt% of catalyst at 220 °C and 4.3 MPa in Scheme 1. The screening tests of the effective catalysts were shown in Fig. 5. It presented the results of 2-aminoethanol reacting with methanol over various catalysts. ZrO₂ catalyst provided poor catalytic activity with 7.3 % selectivity of *N*-methylated products at 12.1 % conversion. B–Zr and Cs–Zr catalysts also exerted unsatisfactory selectivity (11.9 and 3.4 %, respectively) and a moderate conversion (34.1 and 52.4 %, respectively). Nevertheless, Cs–B–Zr catalyst gave the corresponding *N*-alkylation products in moderate to excellent yields for 2-aminoethanol reaction with methanol. Surprisingly, Cs–B–Zr/1 was the best catalyst with the selectivity in the products reached up to 96.3 % with 93.2 % conversion.



Scheme 1 *N*-Alkylation reaction of 2-aminoethanol with methanol over synthesized catalysts

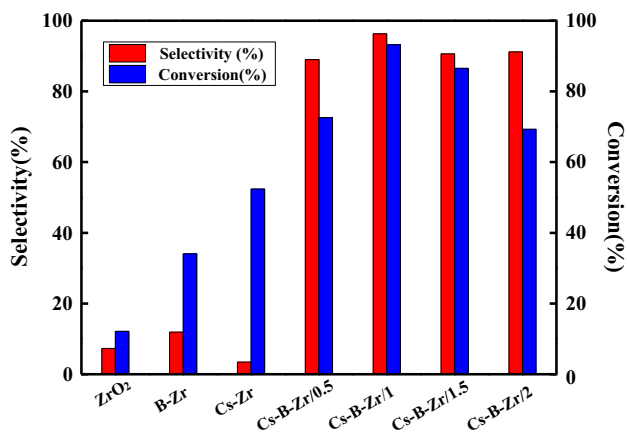


Fig. 5 Reaction of HO (CH₂)₂NH₂ with CH₃OH over various solid catalysts. Conditions: The reaction was conducted at 220 °C and 4.3 MPa in a bath reactor with HO (CH₂)₂NH₂ to CH₃OH molar ratio of 1:3 for 35 min and 4 wt% of catalyst with respect to amine was added

3.5.2 Effect of the Calcined Temperature of Cs–B–Zr/1

Figure 6 showed the effect of calcination temperature on Cs–B–Zr/1 catalytic performance. At the range of 300–550 °C, with the calcined temperature increased, the catalytic activity was gradually improved and achieved the maximum activity at 550 °C. Less activity with sample calcined at temperature less than 550 °C was possibly due to incorporation of CTAB in the sample leading to no formation of a large number of pore structure, which

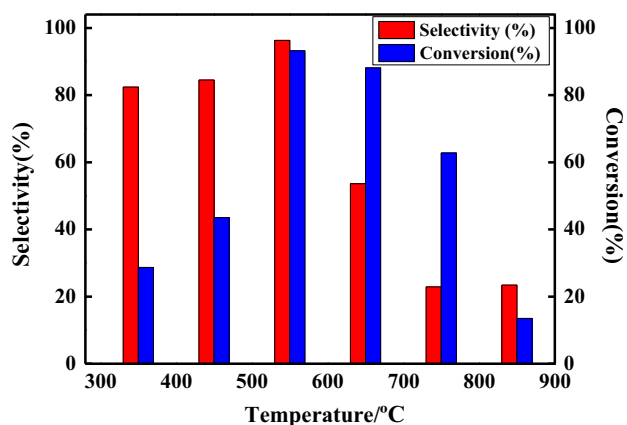


Fig. 6 Effect of the calcined temperature of Cs–B–Zr/1 mixed oxide on the conversion and selectivity under 220 °C and 4.3 MPa for 35 min. Cs–B–Zr/1 was added 4 wt% of catalyst with respect to amine

removed completely after calcination at 550 °C. Nevertheless, the catalytic activity sharply decreased with the temperature further increased over 550 °C. It is believed that with calcination temperature increasing, the formation of the mesoporous structure will collapse and result in lower specific surface area which is responsible for reducing the catalytic activity [42]. XRD and BET results confirmed that the doped amount of boron had an impact on the specific surface area and pore size, which directly affected the catalytic performance of the catalysts [43].

3.5.3 Effect of Reaction Temperature and Reaction Pressure

Figure 7 showed the catalyst performance of the ternary Cs–B–Zr/1 mixed oxide catalyst which was strongly affected by reaction temperature and reaction pressure. As shown in Fig. 7a, the conversion and selectivity were substantially improved when the temperature was above 100 °C, which could reach the highest selectivity of 93.2 % at 220 °C and achieve maximum conversion of 98.4 % at 240 °C. It is well known that the reaction activation energy of the substrate molecular was beyond reach of when the temperature was low. Therefore, the reactions proceed slowly at low temperature, which led to a low conversion. When the temperature further increased ($T > 220$ °C), the selectivity was sharply declined, illustrating side reactions following with the reaction. At higher reaction temperature, the decrease in selectivity was mainly caused by the formation of poly-alkylated products, such as, 2-methoxyethylamine; the dehydration of alcohols or the isomerization of products including the intra- or intermolecular dehydration compounds as byproducts [30]. As shown in Fig. 7b, the *N*-alkylation product yield was also strongly influenced by the reaction pressure. At 0.1–2 MPa, the pressure had little effect on selectivity and conversion (both below 10 %). Increasing the pressure from 2.0 to 4.5 MPa, the conversion and selectivity of the *N*-alkylated products were markedly increased. Noticeably, pressure around at 4.5 MPa, Cs–B–Zr/1 catalyst gave the optimum catalytic activity for *N*-alkylated products with the best conversion of 98.4 % and a total yield of 90.0 %. The conversion and selectivity of *N*-alkylation was observed with a significantly decrease with the pressure further increased over 4.5 MPa. High pressure is helpful for liquefying the reactants (which are low boiling point

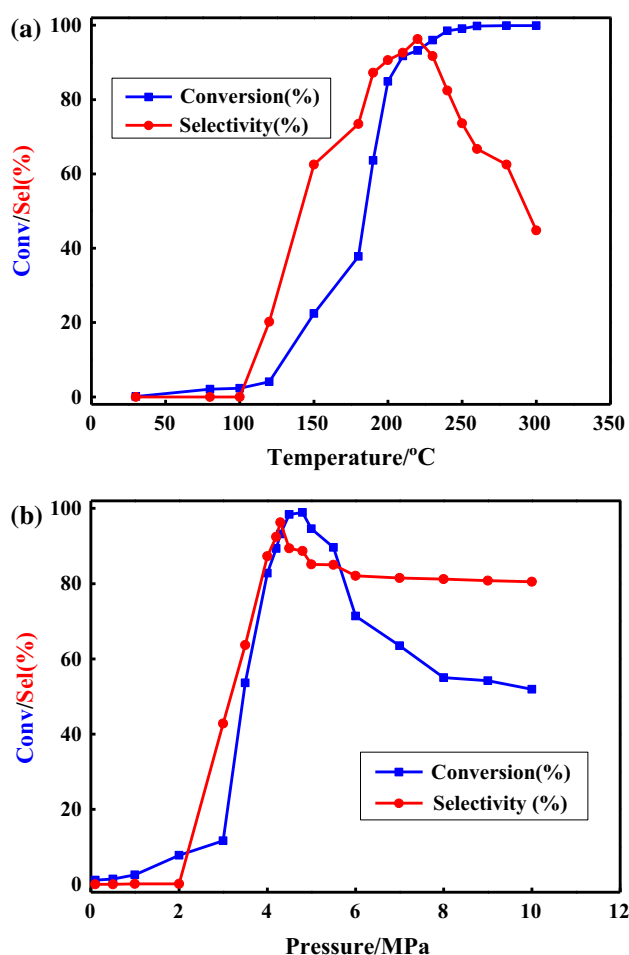


Fig. 7 The conversion and *N*-alkylation selectivity under different conditions: **a** 4.3 MPa for 35 min. **b** 220 °C for 30 min. Conditions: Cs–B–Zr/1 mixed oxide calcined at 550 °C, 4 wt% of catalyst with respect to amine was added, HO(CH₂)₂NH₂:CH₃OH = 1:3

liquids) at high temperature reaction (220 °C) which provide more contact time with catalyst and for adsorption and reaction. Further increase in pressure i.e., after optimum pressure, the reaction was hindered due to detrimental effect on product desorption.

3.5.4 Effect of the Molar Ratio of the Reaction Substrate

The molar ratio of substrate molecules had also a direct impact on the reaction rate, conversion and selectivity for ethanolamine *N*-alkylation. Table 2 summarized the data of the investigation of different molar ratio of amine alcohol reaction with alcohol. The selectivity of *N*-alkylated product was improved by increasing the 2-aminoethanol:methanol molar ratio from 1:1 to 1:20 (73.3–97.4 %, Table 2, entries 1–11). The best conversion result was obtained when the molar ratio of 2-ethanolamine:methanol = 1:3. Cs–B–Zr/1 Catalyst afforded a maximum value of 93.2 % (Table 2, entry 8). Low molar ratio of

2-ethanolamine (less than 1:3) caused a serious drop in conversion (Table 2, entries 10–11) although excess amount of the alcohol was used as a reactant. It could be seen that the *N*-alkylated product selectivity enhanced with decreasing the ratio of amines to methanol from 1:1 to 1:3 and then reached a higher level about 96.3 %. The reason was that high quantity of 2-ethanolamine was responsible for the reduction of selectivity leading to predominantly intermolecular dehydration products, such as piperazine or triethylenediamine [31], which gave poor selectivity in *N*-alkylated product.

3.5.5 Effect of Reaction Substrate

The substrate scope of *N*-alkylation over the Cs–B–Zr mixed-oxide catalysts was investigated at 220 °C and 4.3 MPa with an amine:alcohol molar ratio of 1:3. Table 3 showed the effect of the substitution in the methanol reaction with different functionalized amines in the optimized reaction conditions. Various functionalized amines proceeded to provide the corresponding *N*-alkylated products with different selectivity. Noticeably, it was found that the product yield was influenced by the structures of the amines. An increase in the number of the methylene units in the amino alcohols caused remarkable decrease in the reactivity following the order of 2-aminoethanol > 3-aminopropanol > 5-aminopentanol. Although 4-aminobutanol exhibited good conversion (Table 3, entry 3), it gave predominantly the cyclization product, pyrrolidine, owing to thermodynamic reasons that a high reaction temperature favor the formation of thermodynamically stable six membered cyclization products. It is well-known that molecular dehydration cyclization reaction would be occurred for the alcohol amine to form a ring compound, which made *N*-alkylation product selectivity declined greatly. In sharp contrast to the reactivity of bifunctionalized amines, simple amines such as *n*-butylamine (Table 3, entry 8) or aniline (Table 3, entry 9) were less reactive. It gave the *N*-alkylated products with excellent selectivity regardless of their structures, but with low conversion (10–20 % for the amines). For the linear bifunctionalized amines, the highest conversion and selectivity achieved 93.2 and 96.3 %, respectively (Table 3, entry 1). The results strongly suggested that the hydroxyl group in the functionalized amines was a crucial structural factor to attain excellent reactivity and selectivity.

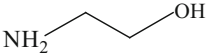
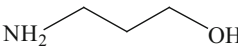
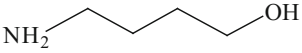
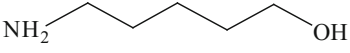
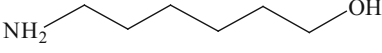
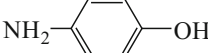
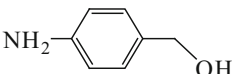
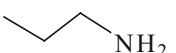
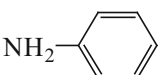
Table 4 showed the effect of the substitution in the 2-aminoethanol reaction with different alcohols in the optimized reaction conditions. A wider range of alcohols, including primary, secondary and tertiary had been substituted with 2-aminoethanol over Cs–B–Zr/1 catalyst. As can be seen from the Table 4, Cs–B–Zr/1 showed the diversity of catalytic effect on different structure alcohol.

Table 2 Effect of the molar ratio of of reaction substrate over the Cs–B–Zr catalyst

Entry	Amine:alcohol (molar ratio)	Conv. (%)	<i>N</i> -Alkylation products sel. (%)
1	1:1	53.6	73.3
2	1:1.1	64.9	75.1
3	1:1.2	69.1	79.8
4	1:1.3	76.7	85.2
5	1:1.5	83.6	88.4
6	1:2	89.3	89.7
7	1:2.5	90.7	92.5
8	1:3	93.2	96.3
9	1:5	90.7	96.9
10	1:10	74.7	97.4
11	1:20	66.5	97.3

Conditions: The reaction was conducted at 220 °C and 4.3 MPa in a bath reactor for 35 min and 4 wt% of a catalyst with respect to amine was added over the Cs–B–Zr/1 Catalyst

Table 3 *N*-Alkylation of various amines over the Cs–B–Zr Catalyst with CH₃OH

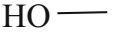
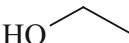
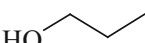
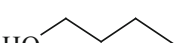
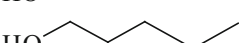
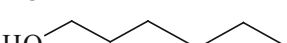
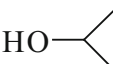
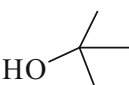
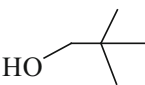
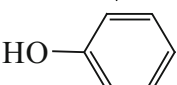
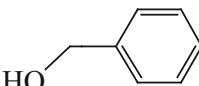
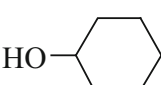
Entry	Amine	Conv. (%)	<i>N</i> -Alkylation products sel. (%)
1		93.2	96.3
2		92.6	95.0
3		91.7	17.4
4		83.9	92.6
5		71.3	87.8
6		52.6	92.7
7		57.4	92.3
8		19.4	94.0
9		15.3	93.6

Conditions: The reaction was conducted over the Cs–B–Zr catalyst at 220 °C and 4.3 MPa in a bath reactor with an amine to CH₃OH molar ratio of 1:3 for 30 min and 4 wt% of catalyst with respect to amine was added

The conversion and selectivity of linear alcohols could reach up around 90 % (Table 4, entries 1–6). While the branched alcohols were relatively low exhibiting comparatively good reactivity and selectivity (77.3 and 89.8 % respectively, Table 4, entry 7). It was found that tertiary alcohols had the worst reactivity over Cs–B–Zr/1 catalyst with poor conversion (32.0 %, Table 4, entry 8). But, the secondary alcohols as the source of the electrophile could give the corresponding tertiary aminoethanol with moderate conversion (77.3 %, Table 4, entry 7). Primary alcohols such as methanol were performed under the same

conditions giving the preferable reactive activity with 96.3 % selectivity and at 93.2 % conversion (Table 4, entry 1). Moreover, steric hindrance also had great effect on the *N*-alkylation reaction process. The marked steric effect of the alkyl substituent on the amino group was demonstrated by the decrease in the reactivity in the order of $-H > -CH_3 > -C_2H_5 > -CH(CH_3)_2 > -C(CH_3)_3$. The catalytic effect on aromatic alcohols such as phenol, benzyl alcohol and cyclohexanol (Table 4, entries 10–12) were far less than aliphatic alcohols, wherein the conversion and selectivity of cyclohexanol were only 15.9 and 21.5 %

Table 4 N-Alkylation of various alcohols over Cs–B–Zr Catalyst with HO(CH₂)₂NH₂

Entry	Alcohol	Conv. (%)	N-Alkylation products sel. (%)
1		93.2	96.3
2		94.0	95.4
3		94.3	95.7
4		92.6	92.4
5		93.8	89.1
6		89.5	91.2
7		77.3	89.8
8		32.0	77.4
9		45.6	82.3
10		24.6	46.2
11		33.2	63.8
12 ^a		15.9	21.5

Conditions: The reaction was conducted over the Cs–B–Zr catalyst at 220 °C and 4.3 MPa in a bath reactor with HO (CH₂)₂NH₂ to an alcohol molar ratio of 1:3 for 30 min and 4 wt% of catalyst with respect to amine was added

^a The molar ratio of HO(CH₂)₂NH₂ to alcohol is 1:2

respectively (Table 4, entry 12). Following the above results, the N-alkylation process had been greatly affected by structure of substrate alcohol.

3.6 Acid–Base Property of the Catalysts

The CO₂/NH₃-TPD was performed to investigate the impact of the catalyst on the N-alkylation reaction process. The CO₂-TPD profiles of the oxide catalyst ZrO₂ and Cs–B–Zr/1 were shown in Fig. 8a. ZrO₂ showed a broad CO₂ desorption peak, including four peaks centered at 250, 425, 510, and 540 °C, which indicated that the surface basic strengths were not homogeneously distributed. In general, the broad CO₂ peaks were divided into two types of desorption peaks, the first broad medium temperature (MT) desorption signal in the range 100–300 °C, corresponding to CO₂ adsorbed on the basic sites at weak strengths and the second broad high-temperature (HT) peak in the range of 300–600 °C, suggesting the presence of very strong

basic sites. In contrast, the MT desorption signals of Cs–B–Zr/1 sharply increased with adding impregnated of boron and cesium suggesting the presence of weak basic sites on the surface of Cs–B–Zr/1. Meanwhile, the peak area of Cs–B–Zr/1 was much higher than ZrO₂ in the same temperature region, which revealed the incorporation of cesium in the mixed oxides system enhancing the total basicity of Cs–B–Zr/1 (Table 5). Borate species do not have any contribution to the basicity except for the fact that increased surface area leads to an increase in basicity [37]. The NH₃-TPD profiles of the oxide catalyst ZrO₂ and Cs–B–Zr/1 were shown in Fig. 8b. ZrO₂ showed two NH₃ desorption peaks at 210 and 410 °C, respectively, which illustrated both the weak acid sites and moderate acid sites on the surface of ZrO₂. Cs–B–Zr/1 showed only a NH₃ desorption peak at 200 °C suggesting only the weak acid sites on the surface of Cs–B–Zr/1. Furthermore, the peak area of Cs–B–Zr/1 was significantly greater than ZrO₂ in the 170–500 °C region indicating the total acidity of Cs–

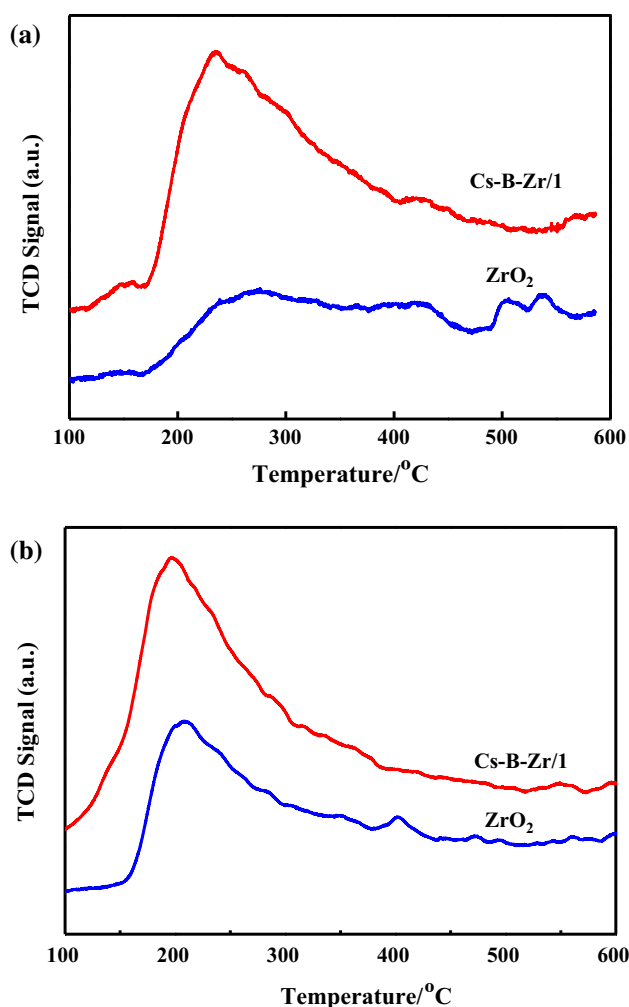


Fig. 8 Patterns of the synthesized materials calcined at 550 °C. **a** CO₂-TPD; **b** NH₃-TPD

Table 5 Total acid amount and basic amount of the synthesized materials

Entry	Samples	Quantity of desorbed gas ($\times 10^{-4}$ mmol/m ²)	
		CO ₂	NH ₃
1	ZrO ₂	153	25
2	B-Zr	235	51.5
3	Cs-B-Zr/0.5	468	46.2
4	Cs-B-Zr/1	850	87.5
5	Cs-B-Zr/1.5	672	67.1
6	Cs-B-Zr/2	539	51.9

The synthesized materials were calcined at 550 °C and determined by CO₂/NH₃-TPD experiment

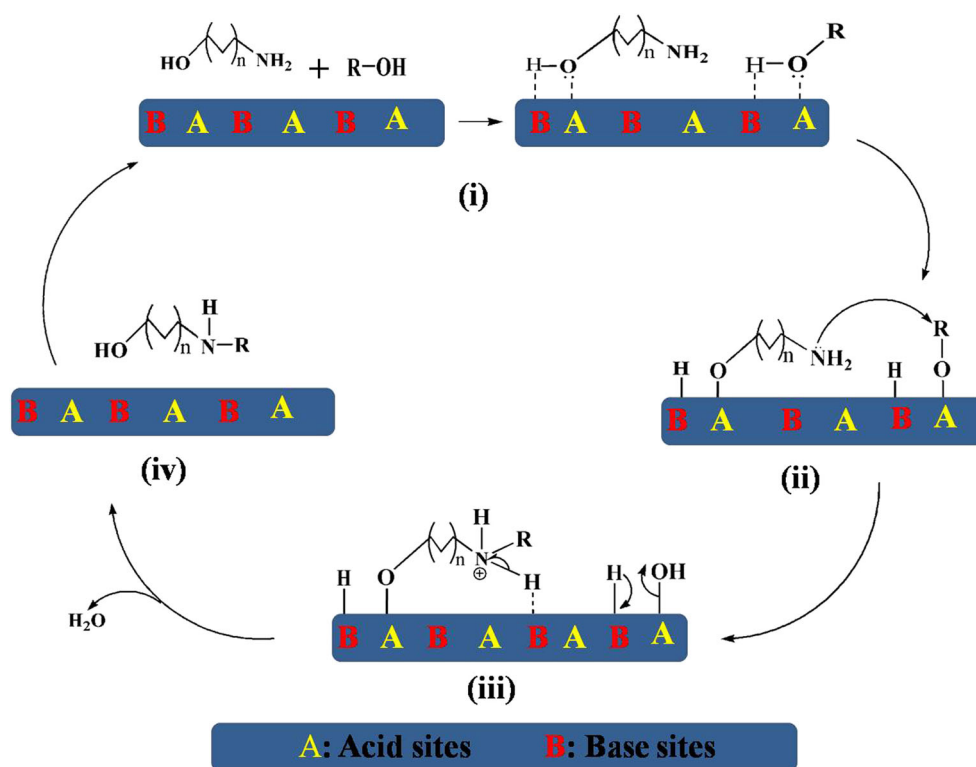
B-Zr/1 was improved (Table 5) by reason of impregnating of boron. This is because that the [BO₃] unit is responsible for the enhancement of acidity, which has an empty orbital and pulls electron cloud from the oxygen of ZrO₂. The

negative charge of boron is diffused into boron oxide bulk by the resonance between the lone pair of oxygen and the empty orbital of boron enhancing the total acidity of the catalyst responsible for better catalytic activity [44]. Table 5 showed total acid amount and basic amount of the synthesized catalysts. It revealed that the total acidity and basicity of the Cs-B-Zr/1 catalyst was improved compared to other catalyst samples. The acidity increased from 0.0025 to 0.0875 mmol m⁻² and basicity from 0.0153 to 0.0850 mmol m⁻². The surface area of the samples also increased from 106 to 227 m² g⁻¹ because of borate and cesium modification (vide supra). The acid-base character of Cs-B-Zr catalyst was directly correlated to the surface area. It increased with surface area because of the increment of accessible active sites, which is responsible for improving the catalytic activity. According to Fig. 5 the results, it could be found that ZrO₂, B-Zr and Cs-Zr exerted unsatisfactory selectivity catalytic activity, however, higher catalytic activity could be obtained over Cs-B-Zr/1 catalyst, which demonstrated that the weak strength acid-basic sites of Cs-B-Zr/1 was much more than other catalysts having a great impact on the conversion and selectivity, which was evidenced by its excellent catalytic performance in the corresponding *N*-alkylation reaction.

3.7 Roles of Cs-B-Zr in *N*-Alkylation Synthesis Process

It is reported that the traditional *N*-alkylation process was employing the borrowing hydrogen strategy [45–47], and some intermediate products, such as aldehyde or imine would appear in the reaction process. Surprisingly, we did not detect any similar intermediate products in our reaction process; thus the reaction mechanism might differ from “B-H” process. Plausible mechanism of the reaction was also illustrated in Scheme 2. (i) The *N*-alkylation reaction proceeded through selective adsorption of alkylamines by the aid of hydroxyl group on the acid–base pair site of the catalyst to lead to the aminoalkyl ester species [48], and alcohols formed its alkyl ester on the neighboring basic and acidic sites in a similar manner; (ii) The amino group in the aminoalkyl ester moieties would exclusively attack the alkyl carbon of the neighboring alkyl ester species on the surface because of the high concentration of alcohols on the catalyst surface. The solvation or local clustering around amino functional group in alcoholamine with alcohol molecules might hinder the intermolecular condensation, leading to the other byproducts [49, 50]; (iii) *N*-alkylation was performed on the aminogroup with alkyl moieties through deprotonation of the amino groups by aid of the basic sites, and the proton on the amino combined with hydroxyl to generate neutral water; (iv) The deprotonation of aminoalkyl ester specie rapidly desorbed from the surface of catalyst in

Scheme 2 Proposed reaction pathway of the acid–base synergetic effect for dehydration on the Cs–B–Zr catalyst surface



conjunction with proton to form alkylamine alcohol. The acid–base pair site could facilitate the first step leading to a better activation of the substrates by the facilitation of the nucleophilic attack at the alkyl ester species in an acid–base cooperative effect. It was the reason why the highest yield of *N*-alkylation of products appeared in the case of Cs–B–Zr mixed oxide (Table 3, entries 1–2). In sharp contrast to the reactivity of bifunctional amines, amine bearing no free hydroxyl group (Table 3, entries 8–9) was less reactive; suggesting that the hydroxyl group of the amino alcohols was a structural factor crucial to determining the high reactivity and selectivity. The amines without hydroxyl as an anchor on the catalyst surface resulted in great differences in the conversion. It is worth noting that higher conversion was obtained from aliphatic amines (Table 3, entries 1–2), not aromatic amine (Table 3, entries 6–7), which both bore amino and hydroxyl groups. It was due to the existence of steric effect in the structure of aromatic amine. Meanwhile, the aromatic group substituents on the amino showed poor nucleophilic substitution performance ordinarily. It was also found that the structure of substrate alcohol (Table 4) was important factor affecting the catalytic activity of the Cs–B–Zr catalyst for the *N*-alkylation of alkylolamines with alcohols. It is known that a nucleophilic substitution of –OH of alcohol by –NH₂ of amines substrate via S_N2 mechanism, and S_N2 transition state would be favored if alcohol is of primary nature (Table 4

entries 1–6). So, secondary and tertiary alcohol (Table 4, entries 7–8) was shown less reactivity. Further studies are essential to gain a better and clearer insight into the mechanism on the overall reaction in our later work.

4 Conclusions

We have demonstrated that Cs–B–Zr mixed oxide catalyst works as an efficient catalyst for the *N*-alkylation of alkylolamines with alcohols providing a very clean process. Cs/B/Zr ratio, calcination temperature, reaction conditions, and reaction substrate had great influence on the catalytic activity of *N*-alkylation of alkylolamines with alcohols. The mechanistic model adequately rationalized the observed reactivity and selectivity. It was revealed that the suitable surface weak acid–base sites, strong interaction between hydroxyl group and the Cs–B–Zr were critical factors leading to excellent catalytic behavior and activity for the *N*-alkylation reaction. The ternary Cs–B–Zr mixed oxide is an attractive alternative catalyst as a cheap and commercially available catalyst in environmentally benign chemical process.

Acknowledgments The authors are grateful for the National Natural Science Foundation of China (Nos. 51002137, 10804099) and the Zhejiang Basic Research Development Program (LQ12E02009).

References

- Lawrence S (2004) Amines: synthesis, properties and application. Cambridge University Press, Cambridge
- Seayad A, Ahmed M, Klein H, Jackstell R, Gross T, Beller M (2002) *Science* 297:1676
- Brown B (1994) The organic chemistry of aliphatic nitrogen compounds. Oxford University Press, New York, pp 350–352
- Yin H, Jin M, Chen W, Chen C, Zheng L, Wei P, Han S (2012) *Tetrahedron Lett* 53:1265
- Lombardo M, Mosconi E, Pasi F, Petrini M, Trombini C (2007) *J Org Chem* 72:1834
- Nakano H, Yokoyama J, Fujita R, Hongo H (2002) *Tetrahedron Lett* 43:7761
- Kashima C, Harada K, Omote Y (1985) *Can J Chem* 63:288
- Chakraborti A, Kondaskar A (2003) *Tetrahedron Lett* 44:8315
- Pujala B, Rana S, Chakraborti A (2011) *J Org Chem* 76:8768
- He W, Wang L, Sun C, Wu K, He S, Chen J, Wu P, Yu Z (2011) *Chem Eur J* 17:13308
- Cui X, Dai X, Deng Y, Shi F (2013) *Chem Eur J* 19:3665
- Jumde V, Gonsalvi L, Guerriero A, Peruzzini M, Taddei M (2015) *Eur J Org Chem* 2015:1829–1833
- Edwards M, Jazzar F, Paine B, Shermer D, Whittlesey M, Williams M, Edney D (2004) *Chem Commun Camb* 1:90
- Grigg R, Mitchell T, Sutthivaiyakit S, Tongpenyai N (1981) *J Chem Soc Chem Commun* 12:611
- Watanabe Y, Tsuji Y, Ohsugi Y (1981) *Tetrahedron Lett* 22:2667
- Hamid M, Allen C, Lamb G, Maxwell A, Maytum H, Watson A, Williams J (2009) *J Am Chem Soc* 131:1766
- Dang T, Ramalingam B, Shan SP, Seayad A (2013) *ACS Catal* 3:2536
- Ohshima T, Miyamoto Y, Ipposhi J, Nakahara Y, Utsunomiya M, Mashima K (2009) *J Am Chem Soc* 131:14317
- Yang H, Mao R, Luo C, Lu C, Cheng G (2014) *Tetrahedron* 70:8829
- Gunanathan C, Milstein D (2008) *Angew Chem Int Ed* 47:8661
- Gnanamgari D, Sauer E, Schley N, Butler C, Incarvito C, Crabtree R (2009) *Organometallics* 28:321
- Kawahara R, Fujita K, Yamaguchi R (2010) *J Am Chem Soc* 132:15108
- Reddy M, Kumar M, Swamy P, Naresh M, Srujana K, Satyanarayana L, Venugopala A, Narender N (2013) *Green Chem* 15:3474
- Tayade K, Mishra M, Munusamy K, Somani R (2014) *J Mol Catal A Chem* 390:91
- Sun Y, Lu X, Wei X, Zhou D, Xia Q (2014) *Catal Commun* 43:213
- Pathare S, Akamanchi K (2013) *Appl Catal A Gen* 452:29
- Lee YY, Kevin WCW (2012) *Phys Chem Chem Phys* 14:13914
- Peng WH, Lee YY, Connie W, Kevin WCW (2012) *J Mater Chem* 22:23181
- Ivanova I, Knyazeva EE (2013) *Chem Soc Rev* 42:3671
- Oku T, Arita Y, Tsuneki H, Ikariya T (2004) *J Am Chem Soc* 126:7368
- Qiu C, Lin T, Zhang Q, Xu HD, Chen Y, Gong M (2011) *Chin J Catal* 32:1227
- Malshe K, Patil P, Umbarkar S, Dongare M (2004) *J Mol Catal A Chem* 212:337
- Kong X, Wang G, Du X, Lu L, Li L, Chen L (2012) *Catal Commun* 27:26–29
- Liang Q, Hu Q, Miao G, Yuan B, Chen X (2015) *Mater Lett* 148:45
- Dayananda D, Sarva V, Prasad S, Arunachalam J, Parameswaran P, Ghosh N (2015) *Appl Surf Sci* 329:1
- Panda A, Sinhamahapatra A, Sutradhar N et al (2011) *Appl Catal A Gen* 402:87
- Panda A, Sinhamahapatra A, Pal P et al (2013) *Chem Cat Chem* 5:331
- Egili K, Oraby A (1996) *J Phys Condens Matter* 8:8959
- Motke S, Yawale S, Yawale S (2002) *Bull Mater Sci* 25:75
- Xu B, Cheng S (1999) S J, Zhu Q. *Appl Catal A Gen* 188:361–368
- Srivastava A, Dongare M (1987) *Mater Lett* 5:111
- Shen W, Tang X, Yong Li et al (2006) *Appl Catal B Environ* 62:265
- Xu S, Hong Y, Chen C, Li S, Xiao L, Fan J (2013) *J Mater Chem A* 1:6191
- Dongare M, Madje B, Patil P et al (2004) *Catal Commun* 5:353
- Xu Q, Li Q, Zhu X, Chen J (2013) *Adv Synth Catal* 355:73
- Lu X, Sun Y, Wei X, Peng C, Zhou D, Xia Q (2014) *Catal Commun* 55:78
- Bahn S, Imm S, Neubert L, Zhang M, Neumann H, Beller M (2011) *ChemCatChem* 3:1853–1864
- Tsuneki H (2001) *Appl Catal A Gen* 221:209
- Wang W, Seiler M, Ivanova I, Sternberg U, Weitkamp J, Hunger M (2002) *J Am Chem Soc* 124:7548
- Wang W, Buchholz A, Seiler M, Hunger M (2003) *J Am Chem Soc* 125:15260